Homeostatic depression shows heightened sensitivity to synaptic calcium

Catherine J. Yeates[1,2,4], C. Andrew Frank[1,2,3]

[1] Department of Anatomy and Cell Biology, University of Iowa Carver College of Medicine, Iowa City, IA, USA

[2] Interdisciplinary Graduate Program in Neuroscience, University of Iowa, Iowa City, IA, USA

[3] Iowa Neuroscience Institute, University of Iowa Carver College of Medicine, Iowa City, IA, USA

[4] Present Address: Department of Biology, University of Dayton, Dayton, OH, USA

*** Correspondence:**
C. Andrew Frank
andy-frank@uiowa.edu

Keywords: synapse, homeostasis, depression, *Drosophila melanogaster*, NMJ, neurotransmission, plasticity

Abstract

Synapses and circuits rely on homeostatic forms of regulation in order to transmit meaningful information. The *Drosophila melanogaster* neuromuscular junction (NMJ) is a well-studied synapse that shows robust homeostatic control of function. Most prior studies of homeostatic plasticity at the NMJ have centered on presynaptic homeostatic potentiation (PHP). PHP happens when postsynaptic muscle neurotransmitter receptors are impaired, triggering retrograde signaling that causes an increase in presynaptic neurotransmitter release. As a result, normal levels of evoked excitation are maintained. The counterpart to PHP at the NMJ is presynaptic homeostatic depression (PHD). Overexpression of the Drosophila vesicular glutamate transporter (VGlut) causes an increase in the amplitude of spontaneous events. PHD happens when the synapse responds to the challenge by decreasing quantal content during evoked neurotransmission – again, resulting in normal levels of postsynaptic excitation.

We hypothesized that there may exist a class of molecules that affects both PHP and PHD. Impairment of any such molecule could hurt a synapse's ability to respond to any significant homeostatic challenge. We conducted an electrophysiology-based screen for blocks of PHD. We did not observe a block of PHD in the genetic conditions screened, but we did find loss-of-function conditions that led to a substantial deficit in evoked amplitude when combined with VGlut overexpression. The conditions causing this phenotype included a double heterozygous loss-of-function condition for genes encoding the inositol trisphosphate receptor (IP_3R – *itpr*) and ryanodine receptor (*RyR*). IP_3Rs and RyRs gate calcium release from intracellular stores. Pharmacological agents targeting IP_3R and RyR recapitulated the genetic losses of these factors, as did lowering calcium levels from other sources. Our data are consistent with the idea that the homeostatic signaling process underlying PHD is especially sensitive to levels of calcium at the presynapse.

1 Introduction

Animal nervous systems use forms of homeostatic synaptic plasticity to maintain stable function. Over the last 20-25 years, studies from diverse systems have revealed a wealth of information about how forms of homeostatic synaptic plasticity are implemented (Davis, 2013; Davis and Müller, 2015; Delvendahl and Müller, 2019; Marder and Goaillard, 2006; Pozo and Goda, 2010; Turrigiano, 2008). In particular, the *Drosophila melanogaster* neuromuscular junction (NMJ) has uncovered many facets of homeostatic implementation on a molecular level (Frank, 2014a; Frank et al., 2020). Much of the NMJ homeostasis work in both Drosophila and vertebrates has focused on a form of homeostatic plasticity termed presynaptic homeostatic potentiation (PHP). With PHP, manipulations that impair postsynaptic muscle receptor function trigger an increase in presynaptic vesicle release (Cull-Candy et al., 1980; Davis et al., 1998; Frank et al., 2006; Petersen et al., 1997; Wang et al., 2016).

Homeostatic plasticity at the NMJ is a bi-directional process. First, PHP is reversible – when manipulations that impair muscle receptor function are removed, the presynaptic potentiation ceases (Wang et al., 2016; Yeates et al., 2017). Second, the Drosophila NMJ can depress quantal content in a homeostatic manner functionally opposite to PHP: Presynaptic homeostatic depression (PHD). Experimentally, one way to trigger PHD is to overexpress the *Drosophila* vesicular glutamate transporter gene, *VGlut,* in motor neurons. Overexpression of the glutamate transporter leads to an increase in the diameter of glutamatergic vesicles, an increase in quantal size across the entire distribution of spontaneous miniature events, and very large spontaneous quantal events (Daniels, 2004). To compensate for this, quantal content at the NMJ is lowered, resulting in normal evoked postsynaptic excitation (Daniels et al., 2004).

Many genes have been shown to be necessary for PHP at the NMJ. But much less is known about PHD. PHP and PHD result in opposite changes in quantal content, and studies suggest divergent and separable mechanisms governing these forms of homeostatic plasticity. Some genes required for homeostatic potentiation are dispensable for homeostatic depression (Gaviño et al., 2015; Li et al., 2018; Marie et al., 2010). Moreover, unlike homeostatic potentiation, homeostatic depression does not appear to involve a change in the size of the readily releasable pool of synaptic vesicles (Li et al., 2018). Rather, homeostatic depression appears to involve a decrease in release probability (Gaviño et al., 2015). Finally, PHP at the NMJ appears to be a process that is dependent on the input (i.e. the type of synapse formed at the NMJ) (Newman et al., 2017) while PHD does not appear to be input specific (Li et al., 2018).

The degree of overlap between homeostatic depression and homeostatic potentiation is unknown. We designed a small-scale, directed screen to test for links between these two forms of homeostatic plasticity. For the screen, we targeted genes based on prior evidence that their impairment in the neuron caused a failure of the long-term maintenance of PHP. We examined loss-of-function conditions for these genes in a VGlut overexpression background for PHD. We did not find any cases of failed homeostatic depression – the conditions we examined showed decreases in quantal content in response to increased quantal size. However, we did find an interesting and unexpected evoked neurotransmission phenotype: a robust decrease in excitatory postsynaptic potential (EPSP) amplitude in a VGlut overexpression background. We observed this phenotype for a double heterozygous loss-of-function condition for the Ryanodine and IP_3 receptors. In our follow-up work, pharmacology phenocopied this genetic result, and our overall findings are consistent with the idea that the PHD system may show a heightened sensitivity to low calcium.

Our findings highlight a novel synaptic transmission phenotype. Prior characterizations of homeostatic depression do not report decreases in EPSP amplitude in VGlut overexpression relative to controls (Daniels et al., 2004; Gaviño et al., 2015; Li et al., 2018; Marie et al., 2010). Studies at the NMJ generally suggest models in which homeostatic compensation maintains evoked neurotransmission at the synapse approximately at control levels (Davis, 2013). Our results suggest that impairing store calcium channels may result in a cumulative defect in neurotransmission when there is a concurrent PHD challenge. We find this interesting, especially in light of the fact that these same store channels are required for the maintenance of PHP (James et al., 2019) and because other recent studies in other systems have implicated store calcium in presynaptic release mechanisms (e.g., (de Juan-Sanz et al., 2017)).

2 Materials and Methods

Drosophila stocks and husbandry

Fruit fly stocks were obtained from the Bloomington Drosophila Stock Center (BDSC, Bloomington, Indiana), Kyoto Stock Center (DGRC, Kyoto, Japan), Japan National Institute of Genetics (Mishima, Shizuoka, Japan), Vienna Drosophila Research Center (VDRC, Vienna, Austria), or from the labs that generated them. w^{1118} was used as a wild-type (WT) control (Hazelrigg et al., 1984). RNAi lines and mutants used in the screen are reported in Supplemental Table S1.

Fruit flies were raised on cornmeal, molasses, and yeast medium (see BDSC website for standard recipe) in temperature-controlled conditions. Animals were reared at 25°C until they reached the wandering third instar larval stage, at which point they were selected for electrophysiological recording. *UAS-VGlut* (Daniels et al., 2004) was recombined with *OK371-GAL4* (Mahr and Aberle,

2006; Meyer and Aberle, 2006) to drive constitutive overexpression of VGlut. The full genotype of these animals is: *w; VGlut, OK371-Gal4/CyO-GFP*. Virgins of these flies were crossed to RNAi lines or mutants to test for changes to homeostatic depression. *w; OK371-Gal4/+* was used as a genetic control for baseline electrophysiology.

Electrophysiology and analysis

Larvae were dissected in a modified HL3 saline comprised of: NaCl (70 mM), KCl (5 mM), $MgCl_2$ (10 mM), $NaHCO_3$ (10 mM), sucrose (115 mM = 3.9%), trehalose (4.2 mM = 0.16%), HEPES (5.0 mM = 0.12%), and $CaCl_2$ (0.5 mM, except as noted).

For pharmacology, Dantrolene (R&D Systems) and Xestospongin C (Abcam) were used. Dantrolene was mixed into saline to a final concentration of 25 µM. Larvae were cut open on the dorsal side and allowed to incubate in the Dantrolene saline for 5 minutes. The rest of the dissection and recording was completed in Dantrolene saline. Xestospongin C was applied in a similar manner, with the animals allowed to incubate in 20 µM Xestospongin C saline for 5 minutes before they were recorded, also in saline containing Xestospongin C.

Electrophysiological data were collected using an Axopatch 200B amplifier (Molecular Devices, Sunnyvale, CA) in bridge mode, digitized using a Digidata 1440A data acquisition system (Molecular Devices), and recorded with pCLAMP 10 acquisition software (Molecular Devices). A Master-8 pulse stimulator (A.M.P. Instruments, Jerusalem, Israel) and an ISO-Flex isolation unit (A.M.P. Instruments) were utilized to deliver 1 ms suprathreshold stimuli to the appropriate segmental nerve. The average spontaneous miniature excitatory postsynaptic potential (mEPSP) amplitude per NMJ was quantified by hand, approximately 100 individual spontaneous release events per NMJ (MiniAnalysis, Synaptosoft, Fort Lee, NJ). Measurements from all NMJs of a given condition were then averaged. For evoked neurotransmission, 30 excitatory postsynaptic potentials (EPSPs) were averaged to find a value for each NMJ. These were then averaged to calculate a value for each condition. Quantal content (QC) was calculated by the ratio of average EPSP and average mEPSP amplitudes for each individual NMJ. An average quantal content was then calculated for each condition. EPSP variability was assessed by measuring each of the 30 traces individually and calculating a standard deviation and range for that NMJ. Range was defined as the maximum EPSP value minus the minimum EPSP value.

Immunostaining

An immunostaining experiment is detailed for Figure 4. Procedures match those previously published (Brusich et al., 2015; Brusich et al., 2018; James et al., 2019; Spring et al., 2016; Yeates et al., 2017). Briefly, third instar larvae were filleted and fixed for 5 minutes with Bouin's fixative (Ricca Chemical, Arlington, TX). After washes, fixed fillets were incubated in primary antibodies overnight at 4ºC, mouse anti-Brp (nc82, 1:250, University of Iowa Developmental Studies Hybridoma Bank) (Wagh et al., 2006) and rabbit anti-Dlg (1:5,000) (Budnik et al., 1996). After washes, fillets were incubated in fluorophore-conjugated secondary antibodies overnight at 4ºC (Jackson ImmunoResearch Labs, West Grove, PA), goat anti-mouse-488 (DyLight, 1:1000) and goat anti-rabbit-549 (DyLight, 1:2000). After washes, fillets were mounted and Dlg boutons were counted blinded by hand and double checked for Brp signal in apposition.

Statistical Analyses

Statistical analyses were conducted using GraphPad Prism Software. Statistical significance was assessed either by Student's T-Test when one experimental data set was being directly compared to a

control data set, or one-way ANOVA with Tukey's post-hoc test when multiple data sets were being compared. Specific p value ranges are noted in the Figure legends and shown in graphs as follows: * $p < 0.05$, ** $p < 0.01$, and *** $p < 0.001$ (* and # are used in Figures if there are additional comparisons highlighted). For some comparisons that are close to $p < 0.05$ statistical significance but do not achieve it ($0.05 < p < 0.1$), specific values are reported on the graph itself. Calcium cooperativity data were analyzed using a non-linear fit regression analysis on GraphPad Prism.

3 Results

A recombinant line to analyze presynaptic homeostatic depression (PHD)

Using previously published reagents, we generated a fly stock with constitutive *VGlut* transgene overexpression. Such a stock could be used as a tool for a single-cross genetic screen. To generate the stock, we recombined the *OK371-Gal4* motor neuron driver (Mahr and Aberle, 2006; Meyer and Aberle, 2006) with a *UAS-VGlut* transgene (Daniels et al., 2004). We placed these two genetic elements in *cis* on *Drosophila melanogaster* Chromosome II. *OK371-Gal4* is an enhancer trap line for the *VGlut* promoter itself. This ensured that GAL4-driven *UAS-VGlut* overexpression would happen in desired tissues, *Drosophila* motor neurons.

We tested if the recombinant line constitutively overexpressing *UAS-VGlut* could express PHD at the NMJ. We crossed the recombinant stock to our wild-type stock (w^{1118}, herein: WT) (Cross result, herein: "*VGlut, OK371/+*"). By NMJ electrophysiology, we recorded from WT control, *OK371/+* control, and *w; VGlut, OK371/+*. As expected, *VGlut, OK371/+* NMJs showed an increase in spontaneous miniature excitatory postsynaptic potential (mEPSP) amplitude compared to controls (Fig. 1A-C; data also in Supplementary Table S1). Compared to WT control NMJs, there was no significant difference in evoked postsynaptic amplitudes for *VGlut, OK371/+* NMJs (Fig. 1D; $p = 0.82$, one-way ANOVA). This was because of an accurate homeostatic decrease in quantal content (QC) (Fig 1E) – hence, successful PHD. This result matched prior studies that had used WT as a control and a *trans OK371/UAS-VGlut* combination to induce PHD (Daniels et al., 2004; Gaviño et al., 2015; Li et al., 2018).

Even though PHD was successful relative to WT for our test cross, we noted a small, but statistically significant, baseline increase in the EPSP amplitude of *OK371/+* NMJs. This increase in *OK371/+* EPSP level was present compared either to WT control or to *VGlut, OK371/+* (Fig. 1D). One possibility is that the *OK371/+* genetic background has slightly elevated release, and the combined addition of *UAS-VGlut* reveals a slight depression in evoked amplitude. Noting this potentially important difference in our driver control, we continued using the *OK371/+* heterozygous condition as a genetic background control. *OK371/+* is a closer genetic control for PHD analysis than WT.

A genetic screen identifies an interaction between calcium stores and a PHD-inducing challenge

We used our recombinant line to conduct a genetic screen for conditions that affect presynaptic homeostatic depression (PHD). We crossed this stock to screen stocks: 1) either to drive *UAS-RNAi* transgenes to knock down genes; 2) to drive other chosen *UAS* transgenes; or 3) to combine with \ heterozygous loss-of-function mutant lines (Materials and Methods, Fig. 2A). For the screen, we targeted a subset of genes previously identified as in the neuron for homeostatic potentiation, or closely related genes. We tested 43 genotypes (sometimes multiple conditions for a single gene), including our homeostatic depression condition, *VGlut, OK371/+* (Fig. 2B, C).

The aggregate results of the screen are reported here (Fig. 2B, C; raw data in Supplementary Table S1). We recorded from 42 experimental heterozygous *mutant/+* or > *UAS-RNAi or -transgene/+* conditions, in the *VGlut, OK371/+* genetic background. Of those 42, 12 achieved EPSPs that were numerically larger than *VGlut, OK371/+*, and 22 achieved QCs that were numerically larger than *VGlut, OK371/+* (Fig. 2B, C). Increased evoked potentials could signify failed PHP – however, none of these cases represented statistically significant increases compared to *VGlut, OK371/+*. None were so much bigger that they were good candidates for "failed PHD." Indeed, all of the candidates had average EPSP and QC levels below *OK371/+* NMJ baseline recordings (Compare Figs 1D, E and Fig. 2B, C).

We noted a phenotype distinct from what we were initially seeking: two crosses yielded larvae with striking decreases in NMJ EPSP amplitudes, more than two standard deviations below the average EPSPs from the baseline *VGlut, OK371/+* data set (Fig. 2B). One case was knockdown of the *Survival motor neuron* (*Smn*) gene with the *UAS-Smn[RNAi]^{JF02057}* line in the *VGlut, OK371/+* background. This was intriguing because Drosophila *Smn* is homologous to human *SMN*. Defects in *SMN* cause Spinal Muscular Atrophy (Lefebvre et al., 1995). Drosophila Smn has been characterized as a potential model for Spinal Muscular Atrophy (Raimer et al., 2020; Sen et al., 2011; Spring et al., 2019). Smn has also previously been implicated in PHP (Sen et al., 2011). However, the result for *UAS-Smn[RNAi]^{JF02057}* was not replicated by other *Smn* knockdown or loss-of-function mutant test crosses (Fig. 2B, C). We did not follow up on *Smn* for this study.

A second case with a striking decrease in EPSP amplitude in the screen was a double heterozygous genetic condition in genes encoding the Drosophila Ryanodine receptor (*RyR*) and inositol 1,4,5-trisphosphate (IP_3) receptor (*itpr*): *VGlut, OK371/RyR^{E4340K}; itpr^{90B}/+* (Fig. 2B, C). Ryanodine receptors (RyRs) and IP_3 receptors (IP_3Rs) are localized to the endoplasmic reticulum. They mediate release of calcium from intracellular stores (Berridge, 1984, 1987, 1998; Simkus and Stricker, 2002). The *RyR^{E4340K}* mutation is a single amino acid substitution (glutamic acid to lysine) (Dockendorff et al., 2000), and the *itpr^{90B}* mutation is a null mutant generated by imprecise excision of a transposon (Venkatesh and Hasan, 1997). We previously defined roles for RyR, IP_3R, IP_3 signaling and upstream components in maintaining presynaptic homeostatic potentiation (PHP) (Brusich et al., 2015; James et al., 2019).

In parallel, we screened single mutant manipulations for both genes. Neither the *RyR^{E4340K}/+* heterozygous condition, nor the *itpr^{90B}/+* heterozygous condition – nor any single heterozygous or RNAi knockdown condition for either gene – yielded as significantly depressed EPSPs in response to PHD challenge (Fig. 2B, C). Therefore, the screen result with the double heterozygote could be due to a genetic interaction, or it could be due to other factors in the genetic background. This preliminary finding required further characterization.

We tested if the electrophysiological phenotype could be due to a baseline neurotransmission defect when both genes are heterozygous. By electrophysiology, we compared NMJs from *OK371/RyR^{E4340K}; itpr^{90B}/+* larvae as a baseline double heterozygous condition vs. NMJs from *VGlut, OK371/RyR^{E4340K}; itpr^{90B}/+* larvae (Fig. 3A-D). Just like WT, the baseline double heterozygous condition did have a slight decrease in EPSP amplitude compared to *OK371/+* driver control (Fig. 3A). This indicated a small, but discernible defect in neurotransmission in animals where the IP_3Rs and RyRs are both impaired. The double heterozygous condition with concurrent *VGlut* gene overexpression showed a further decrease in transmission – compared to its own genetic control, it had increased quantal size (Fig. 3B), but significantly decreased evoked amplitude (Fig. 3C) because of a large decrease in quantal content (Fig. 3D). Finally, the quantal content for *VGlut, OK371/RyR^{E4340K}; itpr^{90B}/+* NMJs was numerically smaller than for *VGlut, OK371/+* NMJs (Fig. 3D), but this latter numerical difference was not statistically significant ($p = 0.07$, one-way ANOVA).

229 We noted that the EPSP amplitude in individual *VGlut, OK371/RyR^{E4340K}; itpr^{90B}/+* NMJ recordings
230 varied markedly from stimulus to stimulus. High variability could indicate unstable neuronal
231 excitability or release. To check if evoked release events were indeed more variable, we completed
232 additional analyses. First, we extracted the amplitude of each individual EPSP event at every NMJ
233 recorded. From these data, we calculated the EPSP standard deviation (S.D.) and coefficient of
234 variation (C.V.) per individual NMJ. We also calculated a range for each NMJ by subtracting the
235 maximum EPSP of the thirty from the minimum. We averaged these S.D., C.V., and range measures
236 for each genotype, considering all of the individual EPSP recordings. For all of these EPSP parameters,
237 *w; VGlut, OK371/RyR^{E4340}; itpr^{90B}/+* animals showed statistically significant higher variability
238 compared to controls (Fig. 3E). By contrast, double heterozygous baseline *OK371/RyR^{E4340K}; itpr^{90B}/+*
239 NMJs did not differ significantly from *w; OK371/+* driver control NMJs ($p > 0.85$ for each measure,
240 Kruskal-Wallis ANOVA), suggesting that the variability stems from *VGlut* overexpression in the
241 mutant background (Fig. 3E). *w; VGlut, OK371/+* NMJs showed numerically higher variability than
242 *w; OK371/+*, but this was not statistically significant (Fig. 3E, $p > 0.25$ for each measure, Kruskal-
243 Wallis ANOVA).

244 Finally, we conducted immunostaining to check if any of these electrophysiological defects might
245 correspond with defects in synaptic growth. We assessed growth by co-staining with antibodies against
246 the postsynaptic PSD-95 homolog, DLG (Budnik et al., 1996) and the presynaptic active zone protein,
247 BRP (Wagh et al., 2006). We counted boutons encased by anti-DLG signal and checked that these
248 boutons were apposed by anti-BRP signal. By this analysis, we saw no significant changes in NMJ
249 growth: neither the PHD challenge; nor the double heterozygous loss of the *RyR/+* and *itpr/+* genes;
250 nor combining those manipulations together yielded significant numerical differences in bouton count
251 ($p > 0.90$ for all comparisons, one-way ANOVA; Fig 4A, B). One caveat to these results is that we
252 only examined these NMJs at the level of bouton count, not at the level of the abundance of specific
253 active zone markers (as in (Böhme et al., 2019; Goel et al., 2019; Gratz et al., 2019)).

254 ***Pharmacology targeting Ryanodine and IP$_3$ receptors recapitulates loss-of-function genetics***

255 We tested if the electrophysiological phenotypes we observed could be recapitulated by combining
256 genetics and pharmacology. We started with the drug Dantrolene. Dantrolene is a RyR antagonist
257 (Vazquez-Martinez et al., 2003; Zhao et al., 2001). In prior work at the *Drosophila* NMJ, we found
258 that application of Dantrolene can abrogate the long-term maintenance of PHP (James et al., 2019).

259 We used a sensitized *OK371/+; itpr^{90B}/+* genetic background. With this background, we could
260 pharmacologically impair RyRs while also genetically impairing IP$_3$Rs. We applied 25μM of
261 Dantrolene to: 1) *OK371/+* NMJs; 2) *VGlut, OK371/+* NMJs; 3) *OK371/+; itpr^{90B}/+* NMJs; and 4)
262 *VGlut, OK371/+; itpr^{90B}/+* NMJs. We also collected a set of data for genetically identical conditions
263 without drug treatment (Fig. 5A).

264 In the absence of drug treatment, PHD proceeded normally (Fig. 5A). We noted that the untreated
265 *OK371/+; itpr^{90B}/+* heterozygous condition had a slightly diminished evoked amplitude compared to
266 *OK371/+* (Fig. 5A, middle). Therefore, the *itpr^{90B}/+* condition could be contributing some
267 neurotransmission loss on its own. But in this case, the addition of *VGlut* transgenic expression to this
268 heterozygous background did not further decrease evoked neurotransmission (Fig. 5A, middle),
269 indicating normal PHP.

270 With 25 μM Dantrolene treatment, we noted that the mEPSP amplitudes were generally smaller than
271 without treatment (compare Figs. 5A, B). Nevertheless, in the *VGlut*-overexpressing backgrounds,
272 mEPSPs were still elevated compared to their respective controls (Fig. 5B). This indicated that in the
273 presence of Dantrolene, there was still homeostatic pressure that could induce PHD. Additionally, with

Dantrolene, EPSP amplitudes in *VGlut*-overexpressing lines were significantly decreased compared to their respective genetic controls (Figs. 5B, C). This was because of a marked decrease in QC (Fig. 5B). In particular, the *VGlut, OK371/+; itpr^{90B}/+* condition (+ Dantrolene) had depressed evoked amplitudes compared either to the *VGlut, OK371/+* (+ Dantrolene) condition or to the *OK371/+; itpr^{90B}/+* (+ Dantrolene) condition (Figs. 5B, C). Collectively, these data could indicate a cumulative neurotransmission defect when impairing both the IP_3Rs and RyRs in a PHD-challenged background.

It is possible that strong impairment of RyRs could be sufficient to cause synthetic phenotypes in conjunction with the PHD regulation system. We ran additional pharmaco-genetic tests using a second sensitized genetic background, *OK371/RyR^{E4340K}* – both with and without drugs and with and without *UAS-VGlut* overexpression. Again, in the absence of pharmacological treatment, PHD proceeded normally in the heterozygous *OK371/RyR^{E4340K}* genetic background (Fig. 6A). With Dantrolene, mEPSPs became significantly larger when *VGlut* was expressed (Fig. 6B, left), but EPSPs were significantly reduced (Figs. 6B, middle, 6D) because of a decrease in quantal content (Fig. 6B, right).

Finally, we attempted the inverse pharmaco-genetic experiment from that in Figure 5. This time we used the IP_3R inhibitor, Xestospongin C (Gafni et al., 1997; Wilcox et al., 1998) and the sensitized *OK371/RyR^{E4340K}* genetic background. We applied 20 µM Xestospongin C, both to *OK371/RyR^{E4340K}* NMJs and to *VGlut, OK371/RyR^{E4340K}* NMJs. mEPSPs were numerically larger when *VGlut* was overexpressed (Fig. 6C, left) – though interestingly, for the Xestospongin C dataset, the data did not achieve statistical significance for mEPSP size ($p = 0.10$, one-way ANOVA). This could indicate only weak to no homeostatic pressure in the presence of Xestospongin C. Nevertheless, EPSPs were significantly reduced (Figs. 6C, middle, 6D) because of a marked decrease in quantal content (Fig. 6C, right).

Taking all of these data together, for each case where we examined a dual impairment of RyR and IP_3R the EPSP amplitudes were all quite low with concomitant VGlut overexpression (Figs. 3, 5, 6).

PHD in very low extracellular calcium

We wondered how impairment of channels that mediate release of calcium from intracellular stores might cause the electrophysiological phenotypes that we observed. It could be the case that they are part of the PHD system. Or it could be the case that impairing these channels does not impinge upon PHD signaling itself – but their loss may sensitize the synapse to additional challenges, such as those brought on by PHD.

Our prior work suggested that these ER calcium store channels and the signaling systems that control them are required to maintain homeostatic potentiation throughout life (Brusich et al., 2015; James et al., 2019). We also found a related result: impairing Ca^{2+} store release mollified hyperexcitability phenotypes caused by gain-of-function Ca_V2 amino-acid substitutions in the alpha1 subunit Cacophony. Ca_V2 channels mediate synaptic calcium influx at the NMJ (Brusich et al., 2018). In light of these prior data, we considered two possibilities for PHD. One model is that the IP_3R and RyR channels play a role in ensuring proper level of neurotransmission coincident with PHD. A different model is that calcium itself plays the important role. If this latter idea were true, it might be the case that lowering calcium influx into the presynaptic terminal would also be sufficient to interact with the PHD signaling process, ultimately lowering evoked transmission.

As a test, we measured release over a range of low extracellular calcium concentrations (0.2-0.5 mM). We examined six genotypes: 1) WT; 2) *w; OK371/+* ; 3) *w; VGlut, OK371/+*; 4) *w; RyR^{E4340K}/+; itpr^{90B}/+*; 5) *w; OK371/RyR^{E4340K} ; itpr^{90B}/+*; and 6) *w; VGlut, OK371/RyR^{E4340K} ; itpr^{90B}/+*. To organize data and to calculate calcium cooperativity, we plotted quantal content as a function of

calcium concentration, with the x-y axes on a log-log scale (Fig. 7A, B). To account for different Ca^{2+} driving forces in the different concentrations, we corrected QC for nonlinear summation in our plots and in our subsequent analyses (NLS Corrected QC) (Martin, 1955).

Non-linear regression analyses revealed that there was no significant difference in calcium cooperativity between any of these genotypes over the range of extracellular [Ca^{2+}] we tested (Fig. 7A, B). The calculated log-log slope values of the control PHD genotypes were: WT (log-log slope = 1.810), *w; OK371/+* (log-log slope = 1.884), and *w; VGlut, OK371/+* (log-log slope = 2.117). Comparing those three slopes with one another by nonlinear regression yielded no significant difference in slope ($p = 0.91$). The log-log slope values of the double heterozygous conditions were: *w;* RyR^{E4340K}*/+ ;* $itpr^{90B}$*/+* (log-log slope = 1.737), *w;* $OK371/RyR^{E4340K}$*;* $itpr^{90B}$*/+* (log-log slope = 2.102), and *w; VGlut,* $OK371/RyR^{E4340K}$ *;* $itpr^{90B}$*/+* (log-log slope = 1.601). Comparing those slopes with one another also yielded no significant difference ($p = 0.77$).

Even though there was no significant difference in calcium cooperativity of release over the range of low [Ca^{2+}] conditions examined, our data did show a very large drop in release between 0.3 and 0.2 mM [Ca^{2+}] – specifically for the genotypes where PHD was induced by *UAS-VGlut* overexpression, or for the genotypes with a double heterozygous impairment of *RyR* and *itpr*. Examining the raw data at 0.2 mM [Ca^{2+}], we observed that there was significant homeostatic pressure for PHD signified by mEPSP amplitude increases in the VGlut-overexpression background (Fig. 7C, left). Yet except for the control NMJs, EPSP amplitudes were very much diminished (Fig. 7C, middle) because of stark drops in QC (Fig. 7C, right).

Together, the data point to two conclusions. First, low extracellular calcium on its own appears to be a case where the synapse experiences a synergistic interaction with PHD challenge (Fig. 7C, *VGlut, OK371/+* data). Second, double heterozygous impairment of *RyR* and *itpr* appears to cause very low levels of baseline release in low calcium, irrespective of PHD challenge (Fig. 7C, middle; compare with Fig. 3C). Taken together, these data suggest that lowering presynaptic calcium by any means (impairing store release and/or impairing influx) is sufficient to impair evoked levels of excitation, in conjunction with a PHD challenge.

PHD challenge interacts with impaired Ca_V2 function

As a final test, we turned back to genetics. Drosophila Ca_V2 channels mediate synaptic calcium influx at the NMJ. We used a hypomorphic mutant in the Ca_V2 alpha1 subunit-encoding *cacophony* gene, cac^S, to limit calcium influx. Ca_V2 is essential for viability, but cac^S hypomorphs are viable and fertile (Kawasaki et al., 2000; Smith et al., 1998). Prior work showed that the cac^S homozygous condition dampens NMJ EPSP amplitude by about 70-80% (Frank et al., 2006); calcium imaging data suggest this is due to a ~50% decrease in Ca^{2+} influx during evoked stimulation (Müller and Davis, 2012). Beyond this phenotype in baseline neurotransmission, cac^S hypomorphs also block PHP expression and PHP-associated increases in presynaptic calcium influx (Frank et al., 2006; Müller and Davis, 2012).

With a single cross, we generated hemizygous cac^S*/Y; VGlut, OK371/+* male larvae (Fig. 8A). Compared to cac^S*/Y* as a baseline mutant control, cac^S*/Y; VGlut, OK371/+* NMJs have a marked increase in mEPSP size (Fig. 8B), indicating homeostatic pressure to induce PHD (Fig. 7B). However, comparing evoked potentials of those two conditions shows that cac^S*/Y; VGlut, OK371/+* NMJs have much smaller EPSPs (Fig. 8C) and a very large decrease in QC (Fig. 8D).

4 Discussion

We began this study in search of genetic conditions that affect PHD (Fig. 2). While we did not find any conditions that result in a block of PHD, we did find conditions that provide insight into how calcium regulation may interact with this form of homeostatic plasticity to affect synapse function. When IP_3R and RyR functions are partially impaired – either by genetics or by pharmacology – the NMJ still executes a PHD-like process. But that process goes beyond what is appropriate for the homeostatic pressure that is applied to the system. As a result, evoked potentials at the NMJ are much smaller than baseline (Figs. 3, 5, 6). A similar phenotype is observed when extracellular [Ca^{2+}] is lowered to 0.2 mM (Fig. 7) and when the Ca_V2 alpha1 subunit gene *cacophony* harbors a hypomorphic mutation, cac^S (Fig. 8).

This phenotype has important implications for proper control of synapse function. Taking our data together, we propose that perturbations that dampen calcium efflux from stores or perturbations that dampen calcium influx from the extracellular environment can both synergistically interact with a PHD challenge to control levels of evoked neurotransmission (Fig. 9).

Screen limitations

We did not identify conditions that blocked PHD, and here we discuss potential limitations of the screen. First, our primary assay was electrophysiology, and we employed a candidate-based method, similar to what has previously been documented in the field for PHP (Frank et al., 2020). By definition, candidate-based screens are limited in scope. Second, we focused on factors previously implicated in the maintenance of PHP function (or closely related signaling factors). The idea was that some factors needed to maintain synaptic homeostasis may be needed to orient the NMJ toward a proper, physiological level of function, regardless of the nature of the homeostatic challenge. This idea could have valence, but it was not guaranteed to produce mutant conditions with greater than normal evoked amplitudes in our screen.

Regarding the electrophysiological data, we did find instances in which the screened EPSP was numerically larger than the baseline for *VGlut, OK371/+*, but no instances identified as "PHD-blocking" (Fig. 2). The *VGlut, OK371/+* baseline evoked potential was high (~35 mV), so it is possible that potential positives at a higher potential could be obscured by the limits of non-linear summation. There were also variations from line to line in resting membrane potential, input resistance, and the degree of mEPSP increase indicative of PHD challenge (Supplementary Table, S1). All of these parameters could contribute to false negatives for the screen. Unless a screen is done to saturation, there will be false negatives. It is important to interpret those parsimoniously. For our screen, we believe the way to interpret a negative is not to state that the screen definitively ruled out a factor – rather, the screen failed to rule in that factor for follow-up study.

Similarities and differences with prior PHD studies at the NMJ

We were able to conduct a PHD screen using our recombinant stock with the *UAS-VGlut* and *OK371-Gal4* elements on the same chromosome. In principle, such a stock can pick up modifier mutations. The trade-off was a simplified, single-generation crossing scheme for genetic screens. Our recombinant stock with the driver and *UAS* elements in *cis* maintains consistent PHD challenge from generation to generation, and it behaves similarly electrophysiologically to *trans OK371/VGlut* combinations used in other studies (Daniels et al., 2004; Gaviño et al., 2015; Li et al., 2018).

There are differences between our study and the findings of other published work. Prior studies have used WT (or w^{1118}) as a control background when compared to VGlut overexpression (Daniels et al., 2004; Gaviño et al., 2015; Li et al., 2018). This is a standard practice. Those studies reported precise

408 PHD when comparing WT vs. *OK371/VGlut* third instar larvae – decreased QC at *OK371/VGlut* NMJs
409 resulting in unchanged evoked transmission. We replicated this finding (Fig. 1). However, we also used
410 our Gal4 driver stock background *OK371/+* as an additional control. For that comparison, we saw a
411 slight depression in the evoked amplitude of *OK371, VGlut/+* NMJs (Fig. 1). One possibility is that
412 our recombinant stock was acting as a sensitized background.

413 A second difference comes from the low extracellular calcium test. A low extracellular calcium
414 experiment was previously done when VGlut overexpression was first characterized (Daniels et al.,
415 2004). For that study, the authors showed that QC was significantly diminished compared to wild-type
416 NMJs by the method of failure analysis. Taking the data of that study in aggregate, the authors
417 concluded that PHD was intact in a variety of conditions, including saline with very low extracellular
418 [Ca^{2+}] (0.23 mM Ca^{2+}, 20 mM Mg^{2+}). Our study may appear to conflict with that study because we
419 found that saline with very low [Ca^{2+}] (0.2 mM Ca^{2+}, 10mM Mg^{2+}) is conducive an interaction with
420 PHD, resulting in low evoked release. One possibility is that since the original study was examining
421 failure percentage vs. WT – and not the absolute value of mEPSPs or EPSPs in low calcium, this might
422 not be as easily observed. Other differences might be attributed genetic background or other
423 differences in recording saline, like magnesium concentration.

424 Finally, one other study previously examined the effects of a cac^S mutation with concomitant VGlut
425 overexpression (Gaviño et al., 2015). The authors did not find the low evoked potentials that we report.
426 The major difference between that experiment and ours is that the prior work examined the cac^S
427 mutation in an extracellular [Ca^{2+}] (1.0 mM) that was double that of our study. The result was a Ca^{2+}
428 driving force that yielded robust baseline EPSPs, even in the cac^S mutant background (Gaviño et al.,
429 2015). Given our results with low calcium concentration (Fig. 7), a similar effect may be at work here.

430

431 ***Known roles for calcium in controlling homeostatic plasticity***

432 The notion that calcium contributes to successful homeostatic signaling is not new. Many roles for
433 voltage-gated calcium channels in synaptic homeostasis are well-documented (Frank, 2014a, b). Prior
434 to our study, there was evidence for voltage-gated calcium channel regulation for both NMJ PHP and
435 PHD. For PHP, loss-of-function conditions in Ca_V2/*cacophony* can impair or block this form of
436 homeostatic regulation (Frank et al., 2006; Frank et al., 2009; Müller and Davis, 2012; Spring et al.,
437 2016). Calcium imaging experiments suggest that the reason is because an increase in calcium influx
438 through Ca_V2 is required for the upregulation of quantal content during PHP, and mutant conditions
439 like cac^S block this increase (Müller and Davis, 2012). Recent studies report that Cacophony and other
440 active zone protein levels increase at the NMJ active zone in response to PHP homeostatic challenges
441 (Böhme et al., 2019; Goel et al., 2019; Gratz et al., 2019). And work from mammalian systems mirrors
442 these findings. For example, with mouse hippocampal cultures, TTX exposure induces a homeostatic
443 decrease in presynaptic calcium influx (Zhao et al., 2011).

444 The converse appears true for PHD. Calcium imaging data from two different studies has shown a
445 decrease in the size of calcium transients at the NMJ in response to presynaptic nerve firing in VGlut-
446 overexpressing animals (Gaviño et al., 2015; Li et al., 2018). The data are mixed on how these
447 decreased transients might come about during PHD. Using a tagged *UAS-cacophony* cDNA transgene,
448 two studies verified that there was a reduction in the amount of GFP-tagged Cacophony alpha1 subunits
449 in Ca_V2 in a VGlut-overexpressing background (Gaviño et al., 2015; Gratz et al., 2019). However, one
450 of these same studies demonstrated that if a tagged genomic construct is used instead, that same Ca_V2
451 reduction is not observed (Gratz et al., 2019). Since the transgenic tagged Cacophony-GFP is the
452 product of a single *cac* splice isoform (Kawasaki et al., 2002; Kawasaki et al., 2004), it could be the

453 case that some isoforms are more dynamically trafficked at the synapse. Another possibility is that
454 existing active zone components are somehow modulated during PHD. Regardless of the actual
455 mechanism, the phenomenon appears conserved: again, with rodent hippocampal preparations,
456 increased neuronal activity through gabazine exposure induces a PHD-like phenomenon ultimately
457 resulting in decreases in calcium influx and release (Jeans et al., 2017; Zhao et al., 2011).

458

459 ***How do calcium stores interact with PHD?***

460 Calcium stores have been studied in the context of neurotransmission and plasticity. We know that
461 endoplasmic reticulum (ER) can be visualized at Drosophila NMJ terminals (Summerville et al., 2016),
462 and recently developed imaging tools employed in multiple systems (including at the Drosophila NMJ)
463 show how nerve stimulation results in dynamic changes to ER lumenal calcium, (de Juan-Sanz et al.,
464 2017; Handler et al., 2019; Oliva et al., 2020). In parallel, other groups working at the Drosophila NMJ
465 have demonstrated important roles in baseline neurotransmission and in PHP for ER resident proteins
466 (Genç et al., 2017; Kikuma et al., 2017). And from our prior work, we know that store calcium channels
467 and upstream signaling components are important for maintaining the NMJ's capacity for PHP
468 throughout life (Brusich et al., 2015; James et al., 2019). We also know that disrupting these same
469 factors can ameliorate hyperexcitability associated with gains of Ca_V2 function (Brusich et al., 2018).
470 Finally, from mammalian work it is clear that IP_3Rs, RyRs, and intracellular calcium govern a variety
471 of forms of neuroplasticity (Berridge, 2016), including paired pulse facilitation (Emptage et al., 2001),
472 and modulation of voltage-gated calcium channel activity (Catterall, 2011; Lee et al., 2000).

473 If PHD were simply a matter of properly functioning neurotransmission machinery, then it is not
474 entirely obvious why PHD would be so sensitive to the amount of calcium available such that evoked
475 release would be impaired greatly either when store-operated channels were impaired or when the
476 amount of influx was lowered. In our study, neurotransmission has not been lowered beyond a point of
477 synapse failure. This means that there is still functional machinery. And PHD, per se, is not disrupted
478 – indeed, there is still depression.

479 With any type of homeostatic system, there not only needs to be error detection (large quantal size) and
480 correction (decreased quantal content), but there also need to be brakes applied to the system to prevent
481 some kind of overcorrection. At first glance, our data could suggest some manner of PHD
482 "overcorrection." In our view, this is an interesting and understudied type of phenomenon that could
483 be examined in many homeostatic systems. But it is also true that the nature of the PHD challenge
484 could simply represent a genetic background that renders the synapse sensitive to any additional insults.

485 So how exactly do levels of calcium (or the function of distinct types of calcium channels found at the
486 synapse) ultimately affect excitation levels? This is a difficult problem. The first step might be to
487 narrow the relevant tissue type(s) involved in PHD signaling. ER and store-operated channels are
488 relevant to the functions of many tissues. In principle, our genetic loss-of-function manipulations to
489 *itpr* and *RyR* could affect store-operated channels either in the neuron or in the muscle or in surrounding
490 tissues like glia. Our pharmacological manipulations using Dantrolene and Xestospongin C could also
491 affect multiple tissue types. Therefore, in principle, changing the levels of cytosolic calcium could
492 either affect local signaling in the neuron, or it could result in aberrant signaling back to the presynaptic
493 neuron, disorienting the homeostat.

494 We favor the idea that the relevant calcium signal is local in the motor neuron for two reasons. First,
495 from our own data, we were able to observe the small evoked neurotransmission phenotype either with
496 manipulations to store calcium or with manipulations that affect presynaptic calcium influx, including
497 partial loss-of-function of neuronal *cacophony*. Second, a recent study puts forth data suggesting that
498 when VGlut overexpression induces PHD, this happens exclusively because of excess presynaptic

glutamate release, and presynaptic depression is initiated independent of any sort of postsynaptic response (Li et al., 2018). Such an autocrine signaling mechanism could very well reveal a role for intracellular calcium signaling in the presynapse.

5 References

Berridge, M.J. (1984). Inositol trisphosphate and diacylglycerol as second messengers. Biochem J *220*, 345-360.

Berridge, M.J. (1987). Inositol trisphosphate and diacylglycerol: two interacting second messengers. Annu Rev Biochem *56*, 159-193.

Berridge, M.J. (1998). Neuronal calcium signaling. Neuron *21*, 13-26.

Berridge, M.J. (2016). The Inositol Trisphosphate/Calcium Signaling Pathway in Health and Disease. Physiol Rev *96*, 1261-1296.

Böhme, M.A., McCarthy, A.W., Grasskamp, A.T., Beuschel, C.B., Goel, P., Jusyte, M., Laber, D., Huang, S., Rey, U., Petzoldt, A.G.*, et al.* (2019). Rapid active zone remodeling consolidates presynaptic potentiation. Nat Commun *10*, 1085.

Brusich, D.J., Spring, A.M., and Frank, C.A. (2015). A single-cross, RNA interference-based genetic tool for examining the long-term maintenance of homeostatic plasticity. Frontiers in cellular neuroscience *9*, 107.

Brusich, D.J., Spring, A.M., James, T.D., Yeates, C.J., Helms, T.H., and Frank, C.A. (2018). Drosophila CaV2 channels harboring human migraine mutations cause synapse hyperexcitability that can be suppressed by inhibition of a Ca2+ store release pathway. PLoS genetics *14*, e1007577.

Budnik, V., Koh, Y.H., Guan, B., Hartmann, B., Hough, C., Woods, D., and Gorczyca, M. (1996). Regulation of synapse structure and function by the Drosophila tumor suppressor gene dlg. Neuron *17*, 627-640.

Catterall, W.A. (2011). Voltage-gated calcium channels. Cold Spring Harbor perspectives in biology *3*, a003947.

Cull-Candy, S.G., Miledi, R., Trautmann, A., and Uchitel, O.D. (1980). On the release of transmitter at normal, myasthenia gravis and myasthenic syndrome affected human end-plates. J Physiol *299*, 621-638.

Daniels, R.W., Collins, C.A., Gelfand, M.V., Dant, J., Brooks, E.S., Krantz, D.E., and DiAntonio, A. (2004). Increased expression of the Drosophila vesicular glutamate transporter leads to excess glutamate release and a compensatory decrease in quantal content. J Neurosci *24*, 10466-10474.

Davis, G.W. (2013). Homeostatic signaling and the stabilization of neural function. Neuron *80*, 718-728.

Davis, G.W., DiAntonio, A., Petersen, S.A., and Goodman, C.S. (1998). Postsynaptic PKA controls quantal size and reveals a retrograde signal that regulates presynaptic transmitter release in Drosophila. Neuron *20*, 305-315.

Davis, G.W., and Müller, M. (2015). Homeostatic control of presynaptic neurotransmitter release. Annu Rev Physiol *77*, 251-270.

537 de Juan-Sanz, J., Holt, G.T., Schreiter, E.R., de Juan, F., Kim, D.S., and Ryan, T.A. (2017). Axonal
538 Endoplasmic Reticulum Ca(2+) Content Controls Release Probability in CNS Nerve Terminals.
539 Neuron *93*, 867-881 e866.

540 Delvendahl, I., and Müller, M. (2019). Homeostatic plasticity-a presynaptic perspective. Curr Opin
541 Neurobiol *54*, 155-162.

542 Dockendorff, T.C., Robertson, S.E., Faulkner, D.L., and Jongens, T.A. (2000). Genetic
543 characterization of the 44D-45B region of the Drosophila melanogaster genome based on an F2 lethal
544 screen. Molecular & general genetics : MGG *263*, 137-143.

545 Emptage, N.J., Reid, C.A., and Fine, A. (2001). Calcium stores in hippocampal synaptic boutons
546 mediate short-term plasticity, store-operated Ca2+ entry, and spontaneous transmitter release. Neuron
547 *29*, 197-208.

548 Frank, C.A. (2014a). Homeostatic plasticity at the Drosophila neuromuscular junction.
549 Neuropharmacology *78*, 63-74.

550 Frank, C.A. (2014b). How voltage-gated calcium channels gate forms of homeostatic synaptic
551 plasticity. Frontiers in cellular neuroscience *8*, 40.

552 Frank, C.A., James, T.D., and Muller, M. (2020). Homeostatic control of Drosophila neuromuscular
553 junction function. Synapse *74*, e22133.

554 Frank, C.A., Kennedy, M.J., Goold, C.P., Marek, K.W., and Davis, G.W. (2006). Mechanisms
555 underlying the rapid induction and sustained expression of synaptic homeostasis. Neuron *52*, 663-
556 677.

557 Frank, C.A., Pielage, J., and Davis, G.W. (2009). A presynaptic homeostatic signaling system
558 composed of the Eph receptor, ephexin, Cdc42, and CaV2.1 calcium channels. Neuron *61*, 556-569.

559 Gafni, J., Munsch, J.A., Lam, T.H., Catlin, M.C., Costa, L.G., Molinski, T.F., and Pessah, I.N.
560 (1997). Xestospongins: potent membrane permeable blockers of the inositol 1,4,5-trisphosphate
561 receptor. Neuron *19*, 723-733.

562 Gaviño, M.A., Ford, K.J., Archila, S., and Davis, G.W. (2015). Homeostatic synaptic depression is
563 achieved through a regulated decrease in presynaptic calcium channel abundance. eLife *4*.

564 Genç, Ö., Dickman, D.K., Ma, W., Tong, A., Fetter, R.D., and Davis, G.W. (2017). MCTP is an ER-
565 resident calcium sensor that stabilizes synaptic transmission and homeostatic plasticity. eLife *6*.

566 Goel, P., Dufour Bergeron, D., Bohme, M.A., Nunnelly, L., Lehmann, M., Buser, C., Walter, A.M.,
567 Sigrist, S.J., and Dickman, D. (2019). Homeostatic scaling of active zone scaffolds maintains global
568 synaptic strength. J Cell Biol *218*, 1706-1724.

569 Gratz, S.J., Goel, P., Bruckner, J.J., Hernandez, R.X., Khateeb, K., Macleod, G.T., Dickman, D., and
570 O'Connor-Giles, K.M. (2019). Endogenous Tagging Reveals Differential Regulation of Ca(2+)
571 Channels at Single Active Zones during Presynaptic Homeostatic Potentiation and Depression. J
572 Neurosci *39*, 2416-2429.

573 Handler, A., Graham, T.G.W., Cohn, R., Morantte, I., Siliciano, A.F., Zeng, J., Li, Y., and Ruta, V.
574 (2019). Distinct Dopamine Receptor Pathways Underlie the Temporal Sensitivity of Associative
575 Learning. Cell *178*, 60-75 e19.

576 Hazelrigg, T., Levis, R., and Rubin, G.M. (1984). Transformation of white locus DNA in drosophila:
577 dosage compensation, zeste interaction, and position effects. Cell *36*, 469-481.

James, T.D., Zwiefelhofer, D.J., and Frank, C.A. (2019). Maintenance of homeostatic plasticity at the Drosophila neuromuscular synapse requires continuous IP3-directed signaling. eLife *8*.

Jeans, A.F., van Heusden, F.C., Al-Mubarak, B., Padamsey, Z., and Emptage, N.J. (2017). Homeostatic Presynaptic Plasticity Is Specifically Regulated by P/Q-type Ca(2+) Channels at Mammalian Hippocampal Synapses. Cell reports *21*, 341-350.

Kawasaki, F., Collins, S.C., and Ordway, R.W. (2002). Synaptic calcium-channel function in Drosophila: analysis and transformation rescue of temperature-sensitive paralytic and lethal mutations of cacophony. J Neurosci *22*, 5856-5864.

Kawasaki, F., Felling, R., and Ordway, R.W. (2000). A temperature-sensitive paralytic mutant defines a primary synaptic calcium channel in Drosophila. J Neurosci *20*, 4885-4889.

Kawasaki, F., Zou, B., Xu, X., and Ordway, R.W. (2004). Active zone localization of presynaptic calcium channels encoded by the cacophony locus of Drosophila. J Neurosci *24*, 282-285.

Kikuma, K., Li, X., Kim, D., Sutter, D., and Dickman, D.K. (2017). Extended Synaptotagmin Localizes to Presynaptic ER and Promotes Neurotransmission and Synaptic Growth in Drosophila. Genetics *207*, 993-1006.

Lee, A., Scheuer, T., and Catterall, W.A. (2000). Ca2+/calmodulin-dependent facilitation and inactivation of P/Q-type Ca2+ channels. J Neurosci *20*, 6830-6838.

Lefebvre, S., Burglen, L., Reboullet, S., Clermont, O., Burlet, P., Viollet, L., Benichou, B., Cruaud, C., Millasseau, P., Zeviani, M.*, et al.* (1995). Identification and characterization of a spinal muscular atrophy-determining gene. Cell *80*, 155-165.

Li, X., Goel, P., Wondolowski, J., Paluch, J., and Dickman, D. (2018). A Glutamate Homeostat Controls the Presynaptic Inhibition of Neurotransmitter Release. Cell reports *23*, 1716-1727.

Mahr, A., and Aberle, H. (2006). The expression pattern of the Drosophila vesicular glutamate transporter: a marker protein for motoneurons and glutamatergic centers in the brain. Gene expression patterns : GEP *6*, 299-309.

Marder, E., and Goaillard, J.M. (2006). Variability, compensation and homeostasis in neuron and network function. Nat Rev Neurosci *7*, 563-574.

Marie, B., Pym, E., Bergquist, S., and Davis, G.W. (2010). Synaptic homeostasis is consolidated by the cell fate gene gooseberry, a Drosophila pax3/7 homolog. J Neurosci *30*, 8071-8082.

Martin, A.R. (1955). A further study of the statistical composition on the end-plate potential. J Physiol *130*, 114-122.

Meyer, F., and Aberle, H. (2006). At the next stop sign turn right: the metalloprotease Tolloid-related 1 controls defasciculation of motor axons in Drosophila. Development *133*, 4035-4044.

Müller, M., and Davis, G.W. (2012). Transsynaptic control of presynaptic Ca(2)(+) influx achieves homeostatic potentiation of neurotransmitter release. Curr Biol *22*, 1102-1108.

Newman, Z.L., Hoagland, A., Aghi, K., Worden, K., Levy, S.L., Son, J.H., Lee, L.P., and Isacoff, E.Y. (2017). Input-Specific Plasticity and Homeostasis at the Drosophila Larval Neuromuscular Junction. Neuron *93*, 1388-1404 e1310.

Oliva, M.K., Perez-Moreno, J.J., O'Shaughnessy, J., Wardill, T.J., and O'Kane, C.J. (2020). Endoplasmic Reticulum Lumenal Indicators in Drosophila Reveal Effects of HSP-Related Mutations on Endoplasmic Reticulum Calcium Dynamics. Front Neurosci *14*, 816.

619 Petersen, S.A., Fetter, R.D., Noordermeer, J.N., Goodman, C.S., and DiAntonio, A. (1997). Genetic
620 analysis of glutamate receptors in Drosophila reveals a retrograde signal regulating presynaptic
621 transmitter release. Neuron *19*, 1237-1248.

622 Pozo, K., and Goda, Y. (2010). Unraveling mechanisms of homeostatic synaptic plasticity. Neuron
623 *66*, 337-351.

624 Raimer, A.C., Singh, S.S., Edula, M.R., Paris-Davila, T., Vandadi, V., Spring, A.M., and Matera,
625 A.G. (2020). Temperature-sensitive spinal muscular atrophy-causing point mutations lead to SMN
626 instability, locomotor defects and premature lethality in Drosophila. Dis Model Mech *13*.

627 Sen, A., Yokokura, T., Kankel, M.W., Dimlich, D.N., Manent, J., Sanyal, S., and Artavanis-
628 Tsakonas, S. (2011). Modeling spinal muscular atrophy in Drosophila links Smn to FGF signaling. J
629 Cell Biol *192*, 481-495.

630 Simkus, C.R., and Stricker, C. (2002). The contribution of intracellular calcium stores to mEPSCs
631 recorded in layer II neurones of rat barrel cortex. J Physiol *545*, 521-535.

632 Smith, L.A., Peixoto, A.A., Kramer, E.M., Villella, A., and Hall, J.C. (1998). Courtship and visual
633 defects of cacophony mutants reveal functional complexity of a calcium-channel alpha1 subunit in
634 Drosophila. Genetics *149*, 1407-1426.

635 Spring, A.M., Brusich, D.J., and Frank, C.A. (2016). C-terminal Src Kinase Gates Homeostatic
636 Synaptic Plasticity and Regulates Fasciclin II Expression at the Drosophila Neuromuscular Junction.
637 PLoS genetics *12*, e1005886.

638 Spring, A.M., Raimer, A.C., Hamilton, C.D., Schillinger, M.J., and Matera, A.G. (2019).
639 Comprehensive Modeling of Spinal Muscular Atrophy in Drosophila melanogaster. Frontiers in
640 molecular neuroscience *12*, 113.

641 Summerville, J.B., Faust, J.F., Fan, E., Pendin, D., Daga, A., Formella, J., Stern, M., and McNew,
642 J.A. (2016). The effects of ER morphology on synaptic structure and function in Drosophila
643 melanogaster. Journal of cell science *129*, 1635-1648.

644 Turrigiano, G.G. (2008). The self-tuning neuron: synaptic scaling of excitatory synapses. Cell *135*,
645 422-435.

646 Vazquez-Martinez, O., Canedo-Merino, R., Diaz-Munoz, M., and Riesgo-Escovar, J.R. (2003).
647 Biochemical characterization, distribution and phylogenetic analysis of Drosophila melanogaster
648 ryanodine and IP3 receptors, and thapsigargin-sensitive Ca2+ ATPase. Journal of cell science *116*,
649 2483-2494.

650 Venkatesh, K., and Hasan, G. (1997). Disruption of the IP3 receptor gene of Drosophila affects larval
651 metamorphosis and ecdysone release. Curr Biol *7*, 500-509.

652 Wagh, D.A., Rasse, T.M., Asan, E., Hofbauer, A., Schwenkert, I., Durrbeck, H., Buchner, S.,
653 Dabauvalle, M.C., Schmidt, M., Qin, G.*, et al.* (2006). Bruchpilot, a protein with homology to
654 ELKS/CAST, is required for structural integrity and function of synaptic active zones in Drosophila.
655 Neuron *49*, 833-844.

656 Wang, X., Pinter, M.J., and Rich, M.M. (2016). Reversible Recruitment of a Homeostatic Reserve
657 Pool of Synaptic Vesicles Underlies Rapid Homeostatic Plasticity of Quantal Content. J Neurosci *36*,
658 828-836.

659 Wilcox, R.A., Primrose, W.U., Nahorski, S.R., and Challiss, R.A. (1998). New developments in the
660 molecular pharmacology of the myo-inositol 1,4,5-trisphosphate receptor. Trends Pharmacol Sci *19*,
661 467-475.

Yeates, C.J., and Frank, C.A. (2020). A class of synaptic signaling molecules required for homeostatic potentiation also tunes homeostatic depression. bioRxiv, 2020.2010.2012.336883.

Yeates, C.J., Zwiefelhofer, D.J., and Frank, C.A. (2017). The Maintenance of Synaptic Homeostasis at the Drosophila Neuromuscular Junction Is Reversible and Sensitive to High Temperature. eNeuro *4*.

Zhao, C., Dreosti, E., and Lagnado, L. (2011). Homeostatic synaptic plasticity through changes in presynaptic calcium influx. J Neurosci *31*, 7492-7496.

Zhao, F., Li, P., Chen, S.R., Louis, C.F., and Fruen, B.R. (2001). Dantrolene inhibition of ryanodine receptor Ca2+ release channels. Molecular mechanism and isoform selectivity. J Biol Chem *276*, 13810-13816.

6 Figure Legends

Figure 1. Presynaptic homeostatic depression (PHD) works successfully with a recombinant line of *OK371-Gal4* and *UAS-VGlut*. (A) NMJ electrophysiological data for miniature excitatory postsynaptic potentials (mEPSP), excitatory postsynaptic potentials (EPSP), and quantal content (QC). Data are normalized to WT (w^{1118}) values. *VGlut, OK371/+* NMJs have increased mEPSP but normal EPSP because of decreased QC, indicative of successful PHD. (*** $p < 0.001$ vs. WT by one-way ANOVA with Tukey's post-hoc). **(B)** Representative electrophysiological traces. Large traces are EPSPs; small traces are mEPSPs. Scale bars for EPSPs (mEPSPs) are 5 mV (1 mV) and 50 ms (1000 ms). **(C)** Raw data for mEPSPs. **(D)** Raw data for EPSPs. **(E)** Raw data for QC. For (C)-(E), bars are averages and error bars are ± SEM. *** $p < 0.001$ vs. WT or vs. *OK371/+*; # $p < 0.05$ vs. *OK371/+*; analyses by one-way ANOVA with Tukey's post-hoc.

Figure 2. An electrophysiology screen in a PHD-challenged genetic background. (A) Crossing scheme for generating larvae for electrophysiological recording. Each animal recorded had a homeostatic challenge provided by VGlut overexpression and a concurrent heterozygous or RNAi condition. **(B)** Data distribution for screened conditions (x-axis = average EPSP for condition; y-axis = average QC for condition). Green = *UAS-VGlut, OK371-Gal4/+*. Red = *UAS-VGlut, OK371-Gal4/RyRE4340K; itpr90B/+*. Purple = *UAS-VGlut, OK371-Gal4/+; UAS-Smn[RNAi]*^{JF02057}*/+*. Dotted line: EPSP value two standard deviations below *UAS-VGlut, OK371-Gal4/+* chosen as a cut off for potential follow-up hits. **(C)** Average EPSPs for screened conditions. All conditions have a *UAS-VGlut, OK371-Gal4/+* genetic background. ">" denotes as *UAS* construct or RNAi line being driven in motor neurons by *OK371-Gal4*. "+" denotes additional mutations present as heterozygotes. Top dotted line denotes *UAS-VGlut, OK371-Gal4/+* average. Bottom dotted line denotes two standard deviations below *UAS-VGlut, OK371-Gal4/+* average.

Figure 3. Double heterozygous loss of the *itpr* and *RyR* genes interacts with the PHD challenge to diminish neurotransmission. Note: Traces and data for *OK371/+* and *VGlut, OK371/+* are repeated from Figure 1, for genetic background comparison. Abbreviations are as in Figure 1. **(A)** NMJ electrophysiological data for mEPSP, EPSP, and QC. Data are normalized to *OK371/+* values. * $p < 0.05$, ** $p < 0.01$, and *** $p < 0.001$ vs. *OK371/+*; ## $p < 0.01$ and ### $p < 0.001$ vs. *OK371/RyRE4340K; itpr90B/+*; analyses by one-way ANOVA with Tukey's post-hoc. **(B)** Raw data for mEPSPs. **(C)** Raw data for EPSPs. **(D)** Raw data for QC. For (B)-(D), bars are averages and error bars are ± SEM. * $p < 0.05$, ** $p < 0.01$, and *** $p < 0.001$ by one-way ANOVA across genotypes,

706 with Tukey's post-hoc. **(E)** Representative electrophysiological traces with standard deviation (S.D.),
707 coefficient of variation (C.V.) and range values for EPSPs. The S.D., C.V., and range were significantly
708 higher for *VGlut, OK371/RyR^{E4340K}; itpr^{90B}/+* vs. its genetic control, *OK371/RyR^{E4340K}; itpr^{90B}/+*. * p
709 < 0.05, ** $p < 0.01$ by one-way ANOVA across genotypes, with Tukey's post-hoc. Scale bars as in
710 Figure 1.
711
712 **Figure 4. No discernible NMJ growth defects.** NMJs of third instar larvae (same genotypes as Figure
713 3) were analysed by immunostaining, co-staining with anti-DLG for the postsynaptic density and anti-
714 Brp to check for apposed presynaptic active zones. **(A)** DLG boutons counted for Segment A2, NMJ
715 6/7. **(B)** DLG boutons counted for Segment A3, NMJ 6/7. No significant differences were found across
716 genotypes ($p > 0.9$ for every possible head-to-head comparison, one-way ANOVA).
717
718 **Figure 5. Genetic impairment of *itpr* combined with pharmacological impairment of RyR**
719 **phenocopies prior genetic findings.** Note: Untreated data for *OK371/+* and *VGlut, OK371/+* are
720 repeated from Figure 1, for genetic background comparison. **(A)** Raw data for mEPSPs (left); raw data
721 for EPSPs (middle); raw data for QC (right) for untreated genotypes as shown; bars are averages and
722 error bars are ± SEM. **(B)** Data as in (A) but with 25 µM Dantrolene added to NMJ preps. * $p < 0.05$,
723 ** $p < 0.01$, and *** $p < 0.001$ by one-way ANOVA with Tukey's post-hoc. **(C)** Representative EPSP
724 traces. Scale bars are as in Figure 1.
725
726 **Figure 6. Additional pharmaco-genetic combinations phenocopy the genetic conditions. (A)** Raw
727 data for mEPSPs (left); raw data for EPSPs (middle); raw data for QC (right) for untreated genotypes
728 as shown; bars are averages and error bars are ± SEM. **(B)** Data as in (A) but with 25 µM Dantrolene
729 added to NMJ preps **(C)** Data as in (A) but with 20 µM Xestospongin C added to NMJ preps. **(D)**
730 Representative EPSP traces. Scale bars are as in Figure 1. * $p < 0.05$, ** $p < 0.01$, and *** $p < 0.001$
731 by Student's T-Test comparing a control dataset (no VGlut overexpression) vs. an experimental dataset
732 (VGlut overexpression).
733
734 **Figure 7. Ca^{2+} concentration-sensitivity of PHD execution. (A)** Log-log plots of recording saline
735 [Ca^{2+}] vs. QC corrected for non-linear summation for WT, *OK371/+*, and *VGlut, OK371/+* conditions.
736 Across the range of [Ca^{2+}] examined, there is no significant difference in calcium cooperativity for
737 these conditions (Nonlinear Regression, $p = 0.91$). **(B)** Data plotted as in (A) but this time with a double
738 heterozygous *RyR^{E4340K}/+; itpr^{90B}/+* genetic background. Across the range of [Ca^{2+}] examined, there
739 is no significant difference in calcium cooperativity for these conditions (Nonlinear Regression, $p =$
740 0.78). **(C)** Raw data for mEPSPs (left); raw data for EPSPs (middle); raw data for QC (right). All data
741 are for the indicated NMJ genotypes in 0.2 mM [Ca^{2+}]; bars are averages and error bars are ± SEM.
742 For mEPSPs, * $p < 0.05$ and *** $p < 0.001$ by Student's T-Test, comparing PHD-challenged genotypes
743 vs. unchallenged genetic controls. For EPSPs and QC, * $p < 0.05$, ** $p < 0.01$, and *** $p < 0.001$ vs.
744 *OK371/+*; ## $p < 0.01$; EPSP and QC analyses done across multiple genotypes by one-way ANOVA
745 with Tukey's post-hoc.
746
747 **Figure 8. Partial impairment of Ca_V2/Cacophony and PHD. (A)** Crossing scheme for generating
748 larvae for electrophysiological recording. Male larvae were hemizygous for the *cac^S* hypomorphic
749 mutation. **(B)** Raw data for mEPSPs. **(C)** Raw data for EPSPs. **(D)** Raw data for QC. For (B)-(D), bars
750 are averages and error bars are ± SEM. * $p < 0.05$, ** $p < 0.01$, and *** $p < 0.001$ by Student's T-Test
751 comparing the control *cac^S* dataset (no *VGlut* overexpression) vs. the experimental *cac^S* dataset (*VGlut*
752 overexpression).
753

754 **Figure 9. Model for how multiple calcium sources interact with the process of PHD.** Under
755 baseline conditions, Ca_V2-type calcium channels contribute to synapse function, as may RyRs and
756 IP_3Rs. Under conditions inducing PHD, synaptic vesicles are enlarged, and QC is decreased, through
757 regulation of sources of calcium. When PHD challenge is coupled with concomitant impairment of
758 RyR and IP_3R channels, evoked potentials are significantly diminished.
759

760 **7 Conflict of Interest**

761 The authors declare that the research was conducted in the absence of any commercial or financial
762 relationships that could be construed as a potential conflict of interest.

763 **8 Author Contributions**

764 C.J.Y. and C.A.F. both did the following: designed research, performed research, analysed data, and
765 wrote and edited the paper.

766 **9 Funding**

767 Funding supporting this work includes an NSF Grant (1557792) and an NIH/NINDS Grant
768 (R01NS085164) to C.A.F. C.J.Y. was supported in part by an NIH/NINDS Predoctoral Training Grant
769 to the University of Iowa (UI) Interdisciplinary Graduate Program in Neuroscience (T32NS007421
770 – PI Daniel T. Tranel), as well as a post-comprehensive exam predoctoral summer fellowship and a
771 Ballard and Seashore Dissertation fellowship via the Graduate College at UI.

772 **10 Acknowledgements**

773 We thank members of the Frank lab for helpful comments. We thank the laboratories of Drs. Tina
774 Tootle, Fang Lin, Toshihiro Kitamoto, Pamela Geyer, and Lori Wallrath for helpful discussions. We
775 also thank Drs. Toshihiro Kitamoto, Joshua Weiner, Christopher Stipp, and Mark Stamnes for helpful
776 feedback on an earlier written version of this study. An earlier version of this manuscript was
777 released as a pre-print at *bioRxiv*, (Yeates and Frank, 2020).

778 **11 Supplementary Material**

779 Please see Supplementary Table S1 for raw data from the electrophysiology screen and a legend
780 explaining the table.

781 **12 Data Availability Statement**

782 The raw data supporting the conclusions in this article will be made available by the authors, without
783 undue reservation.

784

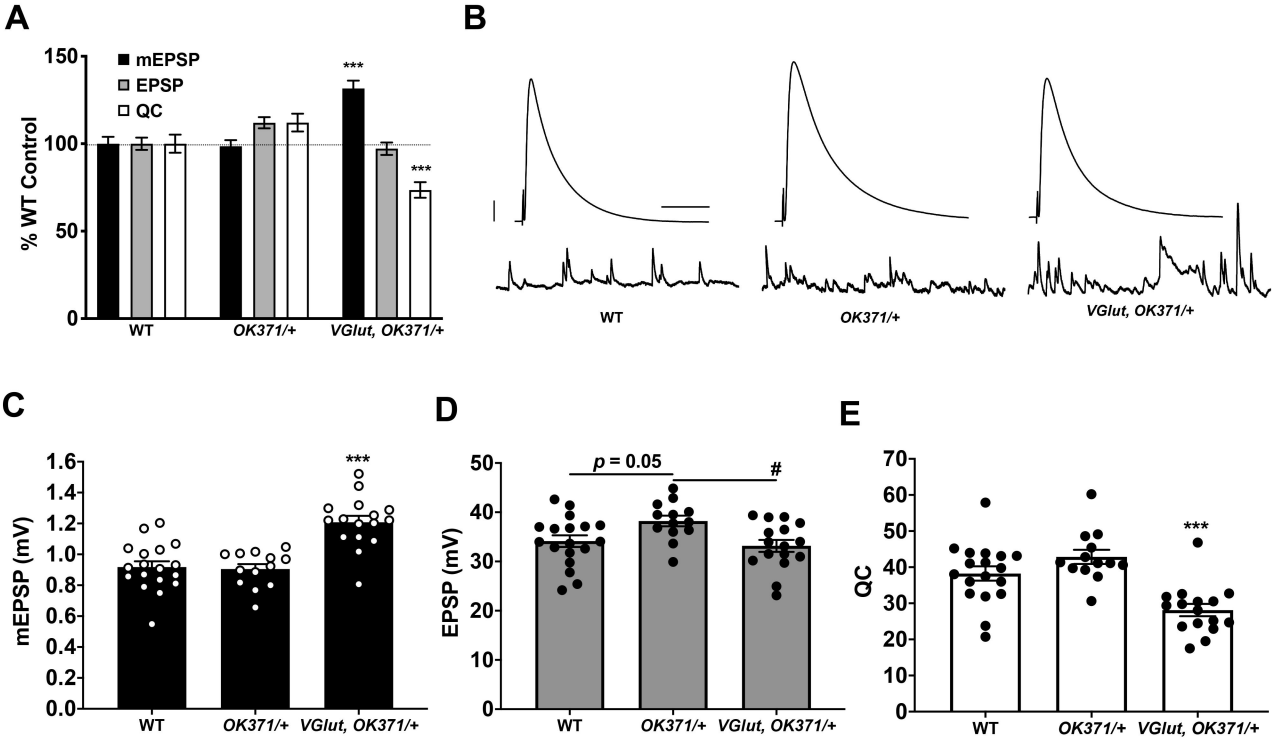
A
mEPSP
EPSP
QC
% WT Control
150
100
50
0
***
***
WT
OK371/+
VGlut, OK371/+
B
WT
OK371/+
VGlut, OK371/+
C
mEPSP (mV)
1.6
1.4
1.2
1.0
0.8
0.6
0.4
0.2
0.0
***
WT
OK371/+
VGlut, OK371/+
D
EPSP (mV)
50
40
30
20
10
0
p = 0.05
#
WT
OK371/+
VGlut, OK371/+
E
QC
70
60
50
40
30
20
10
0
***
WT
OK371/+
VGlut, OK371/+

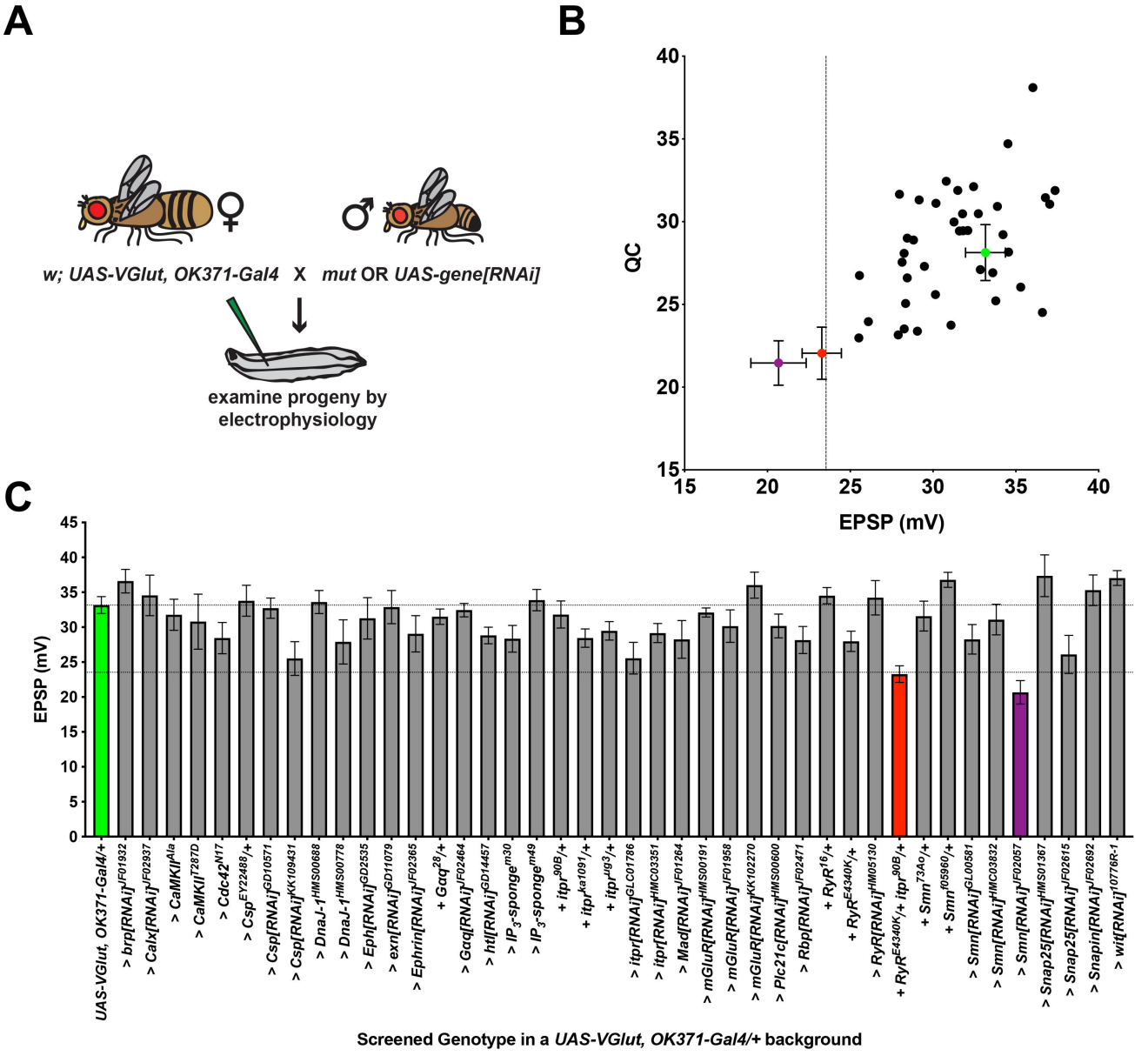
A
w; UAS-VGlut, OK371-Gal4 X mut OR UAS-gene[RNAi]
examine progeny by electrophysiology
B
QC
EPSP (mV)
C
EPSP (mV)
UAS-VGlut, OK371-Gal4/+
> brp[RNAi]JF01932
> Calx[RNAi]JF02937
> CaMKII4a
> CaMKII287D
> Cdc42N17
> CspEY22488/+
> Csp[RNAi]GD10571
> Csp[RNAi]KK109431
> DnaJ-1HMS00688
> DnaJ-1HMS00778
> Eph[RNAi]GD2535
> exn[RNAi]GD11079
> Ephrin[RNAi]JF02365
+ Gαq28/+
> Gαq[RNAi]JF02464
> htl[RNAi]GD14457
> IP3-spongem30
> IP3-spongem49
+ itpr90B/+
+ itprka1091/+
+ itprug3/+
> itpr[RNAi]GLC01786
> itpr[RNAi]HMC03351
> Mad[RNAi]JF01264
> mGluR[RNAi]HMS00191
> mGluR[RNAi]JF01958
> mGluR[RNAi]KK102270
> Plc21c[RNAi]HMS00600
> Rbp[RNAi]JF02471
+ RyR16/+
+ RyRE4340K/+
> RyR[RNAi]HM05130
+ RyRE4340K/+ itpr90B/+
+ Smn73Ao/+
+ Smnf05960/+
> Smn[RNAi]GL00581
> Smn[RNAi]HMC03832
> Smn[RNAi]JF02057
> Snap25[RNAi]HMS01367
> Snap25[RNAi]JF02615
> Snapin[RNAi]JF02692
> wit[RNAi]10776R-1
Screened Genotype in a UAS-VGlut, OK371-Gal4/+ background

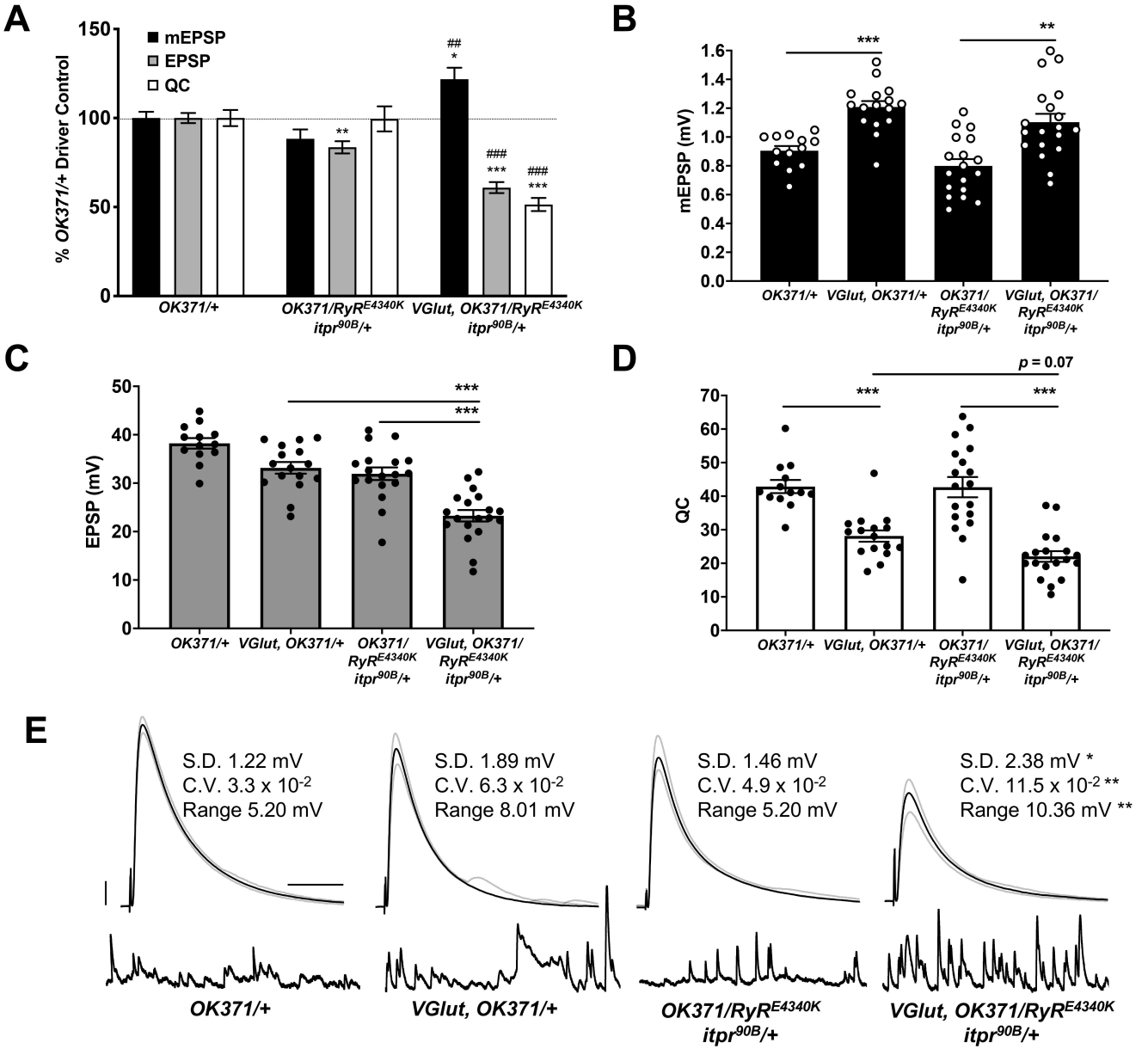
A
mEPSP
EPSP
QC
% OK371/+ Driver Control
150
100
50
0
##
*
**
###
***
***
###
OK371/+
OK371/RyR^{E4340K} itpr^{90B}/+
VGlut, OK371/RyR^{E4340K} itpr^{90B}/+
B
mEPSP (mV)
1.6
1.4
1.2
1.0
0.8
0.6
0.4
0.2
0.0
***
**
OK371/+
VGlut, OK371/+
OK371/ RyR^{E4340K} itpr^{90B}/+
VGlut, OK371/ RyR^{E4340K} itpr^{90B}/+
C
EPSP (mV)
50
40
30
20
10
0
***
***
OK371/+
VGlut, OK371/+
OK371/ RyR^{E4340K} itpr^{90B}/+
VGlut, OK371/ RyR^{E4340K} itpr^{90B}/+
D
p = 0.07
***
***
QC
70
60
50
40
30
20
10
0
OK371/+
VGlut, OK371/+
OK371/ RyR^{E4340K} itpr^{90B}/+
VGlut, OK371/ RyR^{E4340K} itpr^{90B}/+
E
S.D. 1.22 mV
C.V. 3.3 x 10^{-2}
Range 5.20 mV
S.D. 1.89 mV
C.V. 6.3 x 10^{-2}
Range 8.01 mV
S.D. 1.46 mV
C.V. 4.9 x 10^{-2}
Range 5.20 mV
S.D. 2.38 mV *
C.V. 11.5 x 10^{-2} **
Range 10.36 mV **
OK371/+
VGlut, OK371/+
OK371/RyR^{E4340K} itpr^{90B}/+
VGlut, OK371/RyR^{E4340K} itpr^{90B}/+

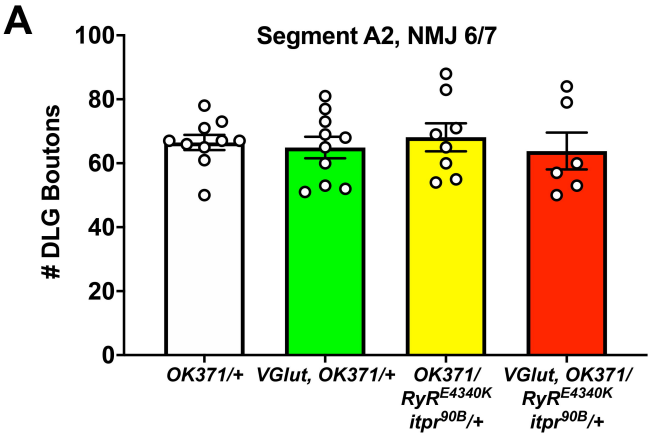
A
Segment A2, NMJ 6/7
DLG Boutons
100
80
60
40
20
0
OK371/+
VGlut, OK371/+
OK371/ RyR^{E4340K} itpr^{90B}/+
VGlut, OK371/ RyR^{E4340K} itpr^{90B}/+

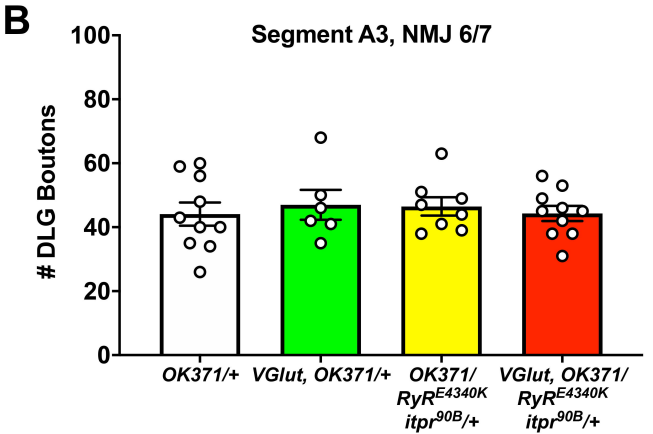
B
Segment A3, NMJ 6/7
DLG Boutons
100
80
60
40
20
0
OK371/+
VGlut, OK371/+
OK371/ RyR^{E4340K} itpr^{90B}/+
VGlut, OK371/ RyR^{E4340K} itpr^{90B}/+

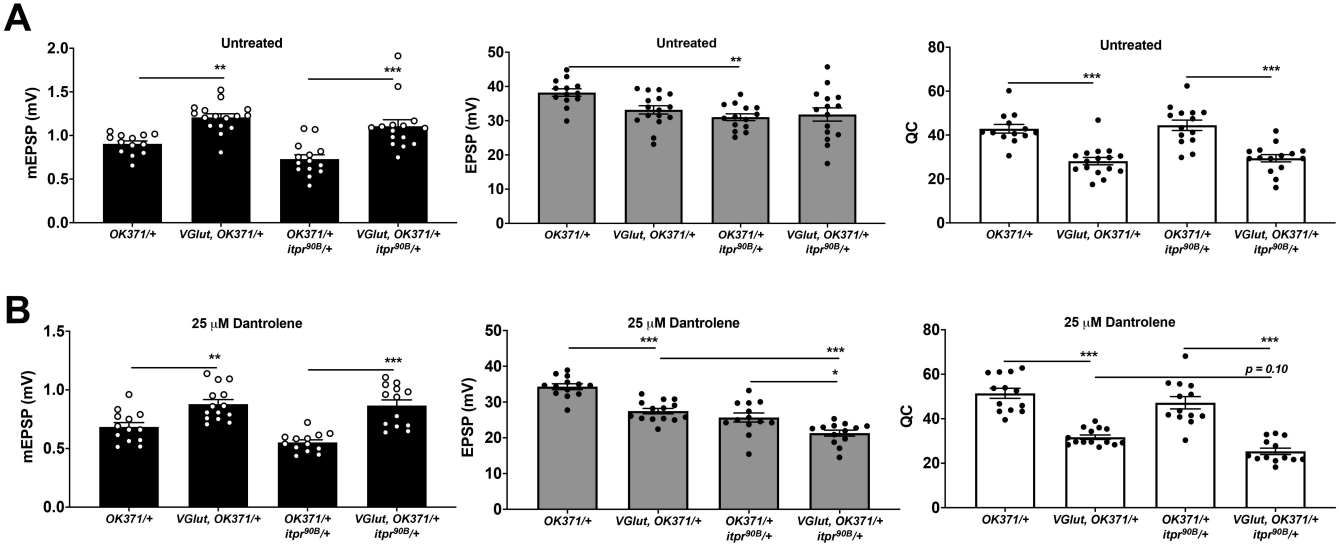
A
Untreated
mEPSP (mV)
2.0
1.5
1.0
0.5
0.0
**
***
OK371/+
VGlut, OK371/+
OK371/+ itpr90B/+
VGlut, OK371/+ itpr90B/+
Untreated
EPSP (mV)
50
40
30
20
10
0
**
OK371/+
VGlut, OK371/+
OK371/+ itpr90B/+
VGlut, OK371/+ itpr90B/+
Untreated
QC
80
60
40
20
0
***
***
OK371/+
VGlut, OK371/+
OK371/+ itpr90B/+
VGlut, OK371/+ itpr90B/+
B
25 μM Dantrolene
mEPSP (mV)
1.5
1.0
0.5
0.0
**
***
OK371/+
VGlut, OK371/+
OK371/+ itpr90B/+
VGlut, OK371/+ itpr90B/+
25 μM Dantrolene
EPSP (mV)
50
40
30
20
10
0
***
***
*
OK371/+
VGlut, OK371/+
OK371/+ itpr90B/+
VGlut, OK371/+ itpr90B/+
25 μM Dantrolene
QC
80
60
40
20
0
***
***
p = 0.10
OK371/+
VGlut, OK371/+
OK371/+ itpr90B/+
VGlut, OK371/+ itpr90B/+
C
25μM Dantrolene
OK371/+
VGlut, OK371/+
OK371/+ itpr90B/+
VGlut, OK371/+ itpr90B/+

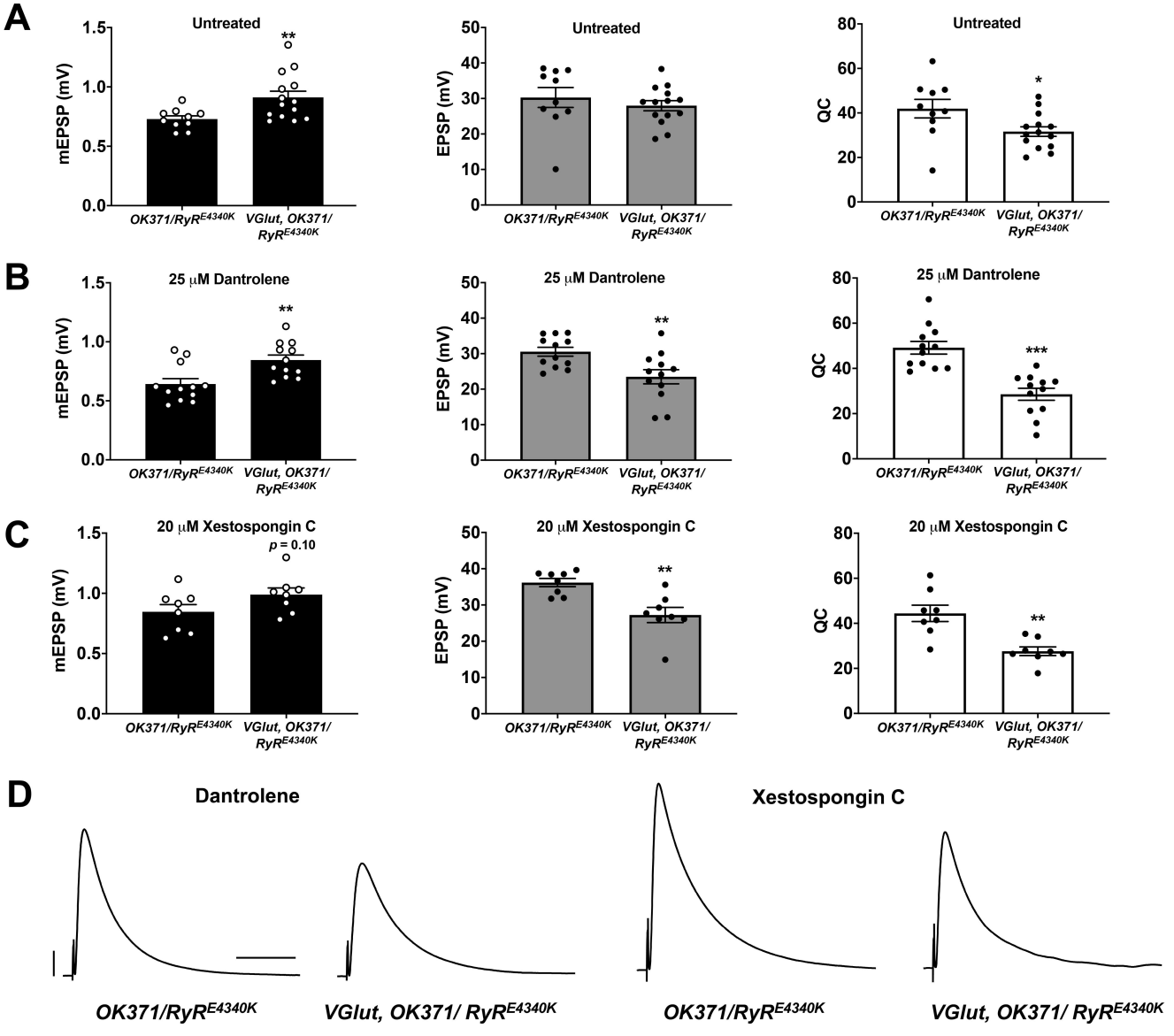
A
Untreated
mEPSP (mV)
1.5
1.0
0.5
0.0
**
OK371/RyR^{E4340K}
VGlut, OK371/ RyR^{E4340K}
Untreated
EPSP (mV)
50
40
30
20
10
0
OK371/RyR^{E4340K}
VGlut, OK371/ RyR^{E4340K}
Untreated
QC
80
60
40
20
0
*
OK371/RyR^{E4340K}
VGlut, OK371/ RyR^{E4340K}
B
25 μM Dantrolene
mEPSP (mV)
1.5
1.0
0.5
0.0
**
OK371/RyR^{E4340K}
VGlut, OK371/ RyR^{E4340K}
25 μM Dantrolene
EPSP (mV)
50
40
30
20
10
0
**
OK371/RyR^{E4340K}
VGlut, OK371/ RyR^{E4340K}
25 μM Dantrolene
QC
80
60
40
20
0
***
OK371/RyR^{E4340K}
VGlut, OK371/ RyR^{E4340K}
C
20 μM Xestospongin C
mEPSP (mV)
1.5
1.0
0.5
0.0
p = 0.10
OK371/RyR^{E4340K}
VGlut, OK371/ RyR^{E4340K}
20 μM Xestospongin C
EPSP (mV)
50
40
30
20
10
0
**
OK371/RyR^{E4340K}
VGlut, OK371/ RyR^{E4340K}
20 μM Xestospongin C
QC
80
60
40
20
0
**
OK371/RyR^{E4340K}
VGlut, OK371/ RyR^{E4340K}
D
Dantrolene
Xestospongin C
OK371/RyR^{E4340K}
VGlut, OK371/ RyR^{E4340K}
OK371/RyR^{E4340K}
VGlut, OK371/ RyR^{E4340K}

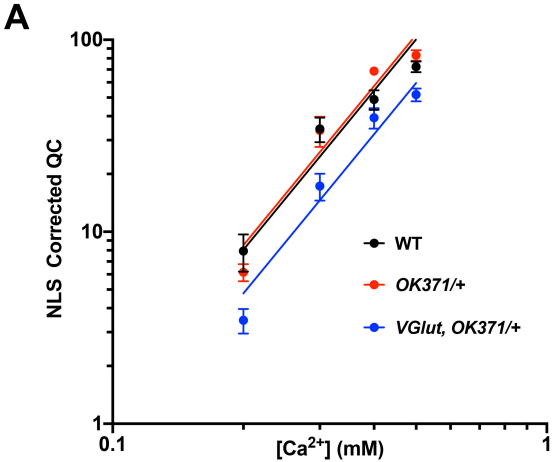
A
NLS Corrected QC
100
10
1
0.1
1
[Ca2+] (mM)
WT
OK371/+
VGlut, OK371/+

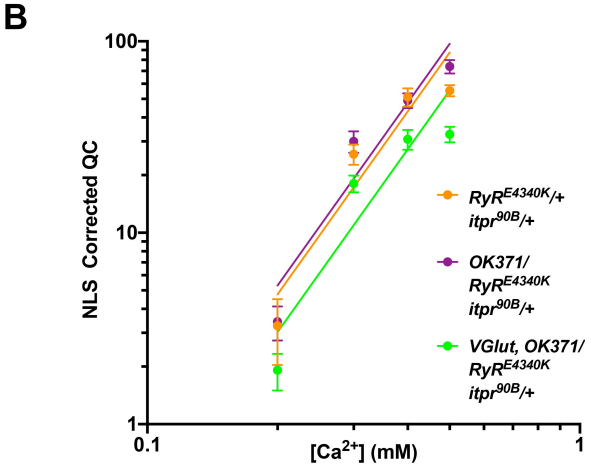
B
NLS Corrected QC
100
10
1
0.1
1
[Ca2+] (mM)
RyRE4340K/+
itpr90B/+
OK371/
RyRE4340K
itpr90B/+
VGlut, OK371/
RyRE4340K
itpr90B/+

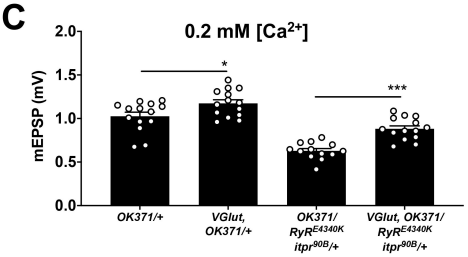
C
0.2 mM [Ca2+]
mEPSP (mV)
2.0
1.5
1.0
0.5
0.0
*
***
OK371/+
VGlut, OK371/+
OK371/ RyRE4340K itpr90B/+
VGlut, OK371/ RyRE4340K itpr90B/+

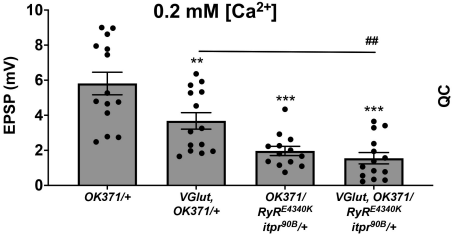
0.2 mM [Ca2+]
EPSP (mV)
10
8
6
4
2
0
##
**
***
***
OK371/+
VGlut, OK371/+
OK371/ RyRE4340K itpr90B/+
VGlut, OK371/ RyRE4340K itpr90B/+

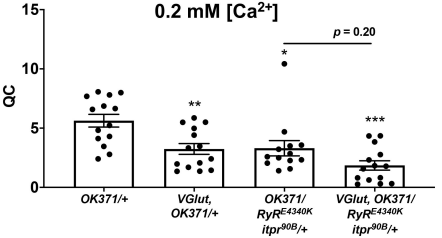
0.2 mM [Ca2+]
QC
15
10
5
0
p = 0.20
*
**
***
OK371/+
VGlut, OK371/+
OK371/ RyRE4340K itpr90B/+
VGlut, OK371/ RyRE4340K itpr90B/+

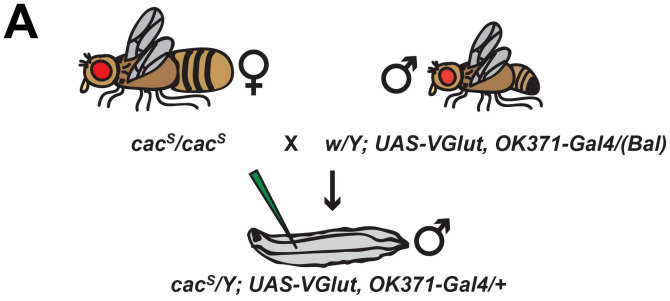
A
cacS/cacS
X
w/Y; UAS-VGlut, OK371-Gal4/(Bal)
cacS/Y; UAS-VGlut, OK371-Gal4/+

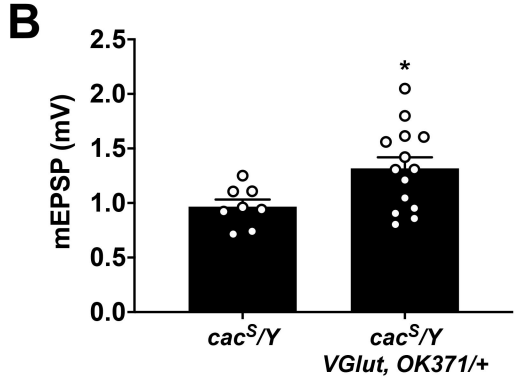
B
mEPSP (mV)
2.5
2.0
1.5
1.0
0.5
0.0
*
cacS/Y
cacS/Y
VGlut, OK371/+

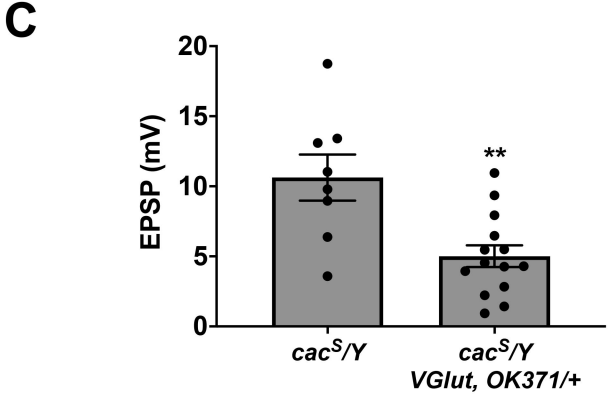
C
EPSP (mV)
20
15
10
5
0
**
cacS/Y
cacS/Y
VGlut, OK371/+

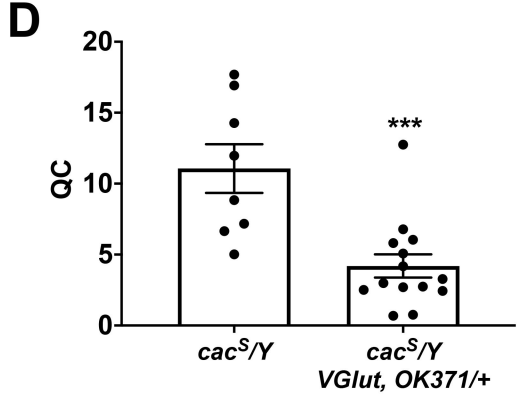
D
QC
20
15
10
5
0
***
cacS/Y
cacS/Y
VGlut, OK371/+

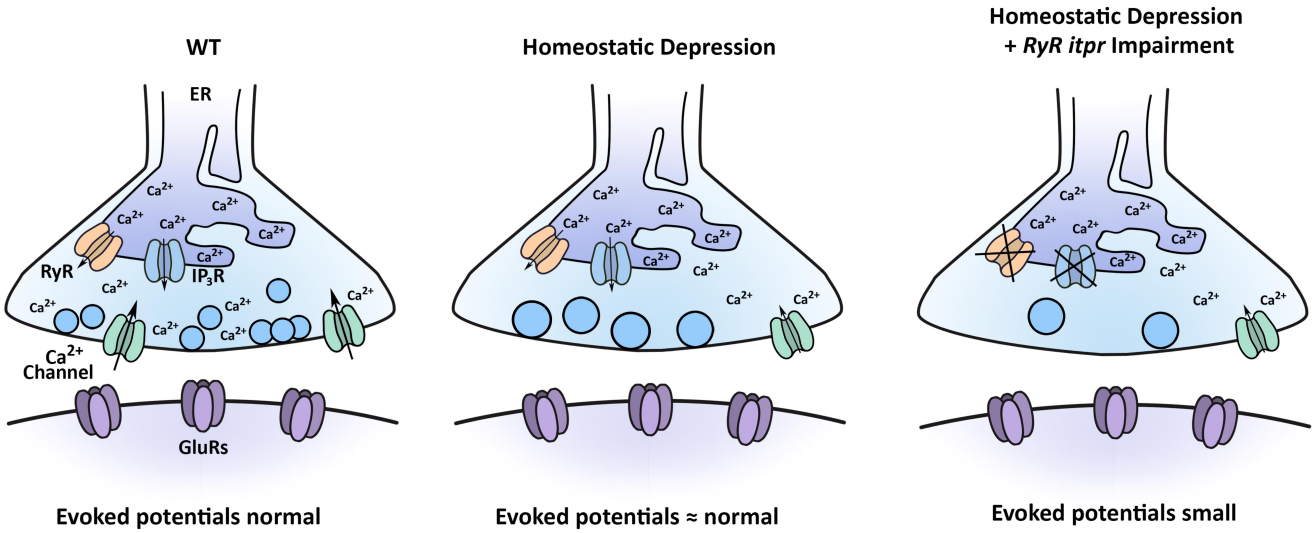
WT
ER
RyR
IP3R
Ca2+
Ca2+ Channel
GluRs
Evoked potentials normal
Homeostatic Depression
Evoked potentials ≈ normal
Homeostatic Depression
+ RyR itpr Impairment
Evoked potentials small